University of Glasgow

Horaruang, W. et al. (2022) Engineering a K+ channel 'sensory antenna' enhances stomatal kinetics, water use efficiency and photosynthesis. *Nature Plants*, 8(11), pp. 1262-1274. (doi: 10.1038/s41477-022-01255-2)

The material cannot be used for any other purpose without further permission of the publisher and is for private use only.

There may be differences between this version and the published version. You are advised to consult the publisher's version if you wish to cite from it.

https://eprints.gla.ac.uk/279300/

Deposited on 13 September 2022

Enlighten – Research publications by members of the University of Glasgow
http://eprints.gla.ac.uk

Engineering a K^+ channel 'sensory antenna' enhances stomatal kinetics, water use efficiency and photosynthesis

Wijitra Horaruang[1,3,4], Martina Klejchová[1,4], William Carroll[1], Fernanda A.L. Silva-Alvim[1], Sakharam Waghmare[1], Maria Papanatsiou[1], Anna Amtmann[1], Adrian Hills[1], Jonas Chaves Alvim[1,5], Michael R. Blatt[1,5,6], and Ben Zhang[2,5]

[1]Laboratory of Plant Physiology and Biophysics, Bower Building, University of Glasgow, Glasgow G12 8QQ. UK

[2]School of Life Sciences, Shanxi University, 92 Wucheng Road, Taiyuan City, Shanxi, China

[3]Current address: Faculty of Science and Arts, Burapha University, Chanthaburi Campus, Chanthaburi Province 22170, Thailand

[4]These authors contributed equally to this research

[5]Co-senior authors

[6]Author for correspondence, email michael.blatt@glasgow.ac.uk

Running title: Engineering native guard cell K^+ channels

Keywords: GORK K^+ channel / ion channel clustering / channel gating, K^+ dependent / photosynthesis / stomatal gas exchange / Arabidopsis

ABSTRACT
Stomata of plant leaves open to enable CO_2 entry for photosynthesis and close to reduce water loss via transpiration. Compared to photosythesis, stomata respond slowly to fluctuating light, reducing assimilation and water use efficiency. Efficiency gains are possible without a cost to photosynthesis if stomatal kinetics can be accelerated. Here we show that clustering of the GORK channel, which mediates K^+ efflux for stomatal closure in the model plant Arabidopsis, arises from binding between the channel voltage sensors, creating an extended 'sensory antenna' for channel gating. Mutants altered in clustering affect channel gating to facilitate K^+ flux, accelerate stomatal movements, and reduce water use without a loss in biomass. Our findings identify the mechanism coupling channel clustering with gating, and they demonstrate the potential for engineering of ion channels native to the guard cell to enhance stomatal kinetics and improve water use efficiency without a cost in carbon fixation.

INTRODUCTION

Stomatal pores form across the epidermal cell layer of plant leaves and are the primary route for CO_2 diffusion from the atmosphere to the mesophyll for photosynthesis. When open, stomata also provide a pathway for water loss from the vapour-saturated environment of the inner air space of the leaf to the atmosphere. As a consequence, stomata must frequently balance the need for CO_2 in photosynthesis against the need to prevent drying of the leaf. Stomata can limit photosynthetic rates by 50% or more when the demand for CO_2 outstrips the capacity for water delivery to the leaf[1,2].

Not surprisingly, stomata connect global water and carbon cycles, impacting both, and are a key factor in weather prediction[3,4]. They are widely recognized to lie at the center of the crisis in fresh water availability and crop production that is expected over the next 20-30 years[5]. Much research to reduce the water used by crops has focused on reducing stomatal density, despite its implicit penalty for photosynthetic assimilation[2]. Circumventing this carbon:water trade-off poses a different set of challenges that are best addressed by altering stomatal aperture dynamics.

Stomatal aperture is controlled by the turgidity of the guard cells surrounding the pore. Guard cells respond to changes in light and CO_2 within the leaf, to atmospheric relative humidity, and to the water-stress hormone abscisic acid; they transport solutes, especially K^+ salts, and water across the plasma membrane to adjust cell turgor[6,7]. Guard cell H^+-ATPases generate an electrochemical potential difference for H^+ and a membrane voltage, negative inside, that facilitates K^+ uptake through K^+ channels, in Arabidopsis primarily KAT1[8-11] and high-affinity K^+ transport[12-15]. Stomata close when reduced H^+ pumping and the activation of Cl^- channels combine to depolarize the plasma membrane thereby promoting K^+ and Cl^- efflux from the guard cells.

A major pathway for K^+ efflux is the GORK K^+ channel and its elimination in the *gork* null mutant slows stomatal closure[16,17]. Like other K^+ channels mediating K^+ efflux in plant cells, GORK channel activation - so-called gating - is inhibited by extracellular K^+ and promoted by depolarizing membrane voltage[6,18,19]. In parallel, GORK assembles clusters at the plasma membrane. Previous studies showed that GORK retains its gating characteristics when expressed heterologously, and these characteristics parallel those of supramolecular channel clustering[16,17,20]: GORK assembled clusters at submillimolar K^+ that reversibly disassembled when K^+ was raised to 10 mM and higher concentrations; additionally, clustering was inhibited by the K^+ channel blocker Ba^{2+} that enters and lodges in the channel pore, preventing K^+ permeation and blocking conformational relaxation to the closed state[20]. Thus, clustering and gating appeared connected as characteristics intrinsic to the GORK protein itself.

We examined the clustering of GORK to assess its mechanistic connection to the voltage- and K^+-dependencies of channel gating. Here we report that clustering arises from a unique set of interactions between charged surfaces of neighboring voltage sensor domains that surround the central pore of each GORK K^+ channel. These interactions extend a 'sensory antenna' network that adjusts channel activity with external K^+. Manipulating the binding surfaces uncouples GORK activity from clustering to promote channel activity. We have used this knowledge to engineer channels modified in gating and enhance guard cell K^+ flux. We show that the cluster-suppressed channels accelerate stomatal closure and enhance stomatal kinetics and aperture. The findings offer a strategy for enhancing plant water use efficiency and photosynthetic carbon assimilation by engineering transport native to the guard cells.

RESULTS

GORK channels interact via the voltage-sensor domain N-terminus

The outward-rectifying channel GORK – like the closely-related channel SKOR[17,21,22] and inward-rectifying channel KAT1[23,24] in Arabidopsis – belongs to the superfamily of voltage-gated K^+ channels that are found across all phyla[25-29]. These proteins form functional channels as tetramers, each protein subunit comprising six transmembrane α-helices with cytosolic N- and C-termini (Fig. 1a). The first four α-helices (S1-S4) of the subunit form a semi-autonomous voltage-sensor domain (VSD), a structure that is highly conserved among voltage-gated channels[30]. The last two α-helices (S5-S6) line a water-filled pore through the membrane at the center of the tetrameric channel assembly. The pore-lining α-helices connect to the VSD through a cytosolic linker and interactions between the S4 and S5 α-helices, ensuring that conformational changes between the VSD and the pore occur in 'lockstep'. The VSD itself incorporates a network of charges that, with a change in voltage, drive VSD conformation and favor the open channel pore[30-32].

Within the plane of the membrane, the VSDs form an outer ring around the channel pore (Fig. 1a). We reasoned therefore that clustering between GORK channels within the membrane was likely to entail inter-channel interactions between VSDs. Of course, the individual subunits of a K^+ channel will interact through the pore-lining α-helices when assembled in the functional channel, but this should not be true of the VSD alone. Thus, we generated VSDs to test whether these truncated channel domains would interact with the full-length channel protein, knowing that VSDs are expressed on their own in the membrane[33].

We used the yeast mating-based split-ubiquitin screen (mbSUS) to test for interactions. mbSUS enables tests with full-length membrane proteins and yields growth of the diploid yeast on selective media only when the two halves of the split-ubiquitin moiety are brought together through interaction between putative protein interactors to which they are fused[33-35]. Strong growth was recovered on selective media, even in 500 μM Met that suppresses bait expression, but growth was not recovered with the VSD of KAT1 (kVSD) or with full-length KAT1 as preys (Fig. 1b). Diploid yeast expressing full-length KAT1 as bait also failed to grow with the full-length GORK, GORK VSD (gVSD), and kVSD as preys, although KAT1 interacted with itself consistent with the tetrameric assembly of the full-length channels (Supplemental Fig. 1). These findings demonstrated an interaction with GORK that was specific to the structure of the gVSD.

Interaction depends on a surface of alternating charged residues

We carried out sequential domain substitutions in gVSD with the corresponding domains of kVSD (Supplemental Fig. 2) in order to identify regions critical for gVSD interaction with GORK. Again, the VSD-GORK interactions were tested by mbSUS assay. Growth of the diploid yeast (Fig. 1c) in the presence of Met was recovered with chimeras that incorporated the cytosolic N-terminus of gVSD, even when the remaining structure was from kVSD. Conversely, interaction was strongly reduced when the N-terminus of gVSD was replaced with the kVSD N-terminus. Some growth was evident without added Met when yeast expressed the kVSD N-terminus in the GORK VSD backbone, specifically with the $gVSD^{kNgS1\text{-}L4}$ and $gVSD^{kN\text{-}L1gS2\text{-}L4}$ preys. This weaker growth was lost when the N-terminus and the cytosolic S2-S3 loop of the gVSD backbone were both replaced with the corresponding kVSD sequences, suggesting the presence of an internal binding site for the VSD N-terminus of the full-

length GORK, possibly in the GORK S2-S3 loop. We concluded that the primary site essential for binding was localized within the cytosolic N-terminus of 69 residues of the GORK channel.

Both the GORK and KAT1 N-termini harbor similarly charged amino acids in the first 21 residues, diverging thereafter before converging to a near-identical sequence near the base of the S1 α-helix (Supplemental Fig. 2). Deleting the first 23 residues of the gVSD N-terminus had no obvious effect on its interaction with GORK in mbSUS assays, but further truncations failed to recover yeast growth (Supplemental Fig. 3) indicating that residues critical for interaction were situated among the subsequent 39 amino acids preceding the S1 α-helix. However, alanine-scanning mutagenesis of residues 23-66, individually and severally among the most divergent regions within this sequence (Supplemental Figs. 4 and 5), failed to uncover a clear difference in yeast growth, suggesting that interactions between the VSD N-termini of GORK did not depend on a unique amino acid motif.

GORK is a member of the cyclic nucleotide-binding domain subfamily of K^+ channels that includes all of the plant K^+ channels with six transmembrane α-helices[25,26]. Alligning the N-termini of GORK and related channels of species from *Brassica napus* to wheat and rice showed a pattern of alternating charged regions (Fig. 2a) that is retained among a subset of known and putative GORK homologs and is not evident in channels of *Sellaginella, Physcomitrella* and *Chlamydomonas* nor in inward-rectifying K^+ channels such as KAT1 and AKT1. We reasoned that this alternation might present a charged surface 'registered' for a zipper-like interaction of the gVSD N-terminus with a complementary surface on the full-length channel. Indeed, replacing all negatively-charged amino acids (Asp, Glu) with positively-charged residues (Lys) within these domains ($gVSD^{NP}$) suppressed diploid yeast growth in split-ubiquitin assays; growth was similarly suppressed when all positively-charged residues were replaced with negatively-charged residues ($gVSD^{PN}$) and when all of the charged residues were substituted with Ala. ($gVSD^{A}$). However, growth was recovered (Fig. 2c) when negatively- and positively-charged residues were exchanged ($gVSD^{PNNP}$).

To support these findings, we carried out gel filtration analysis for N-terminal multimer assemblies in vitro and assessed VSD-GORK interaction by ratiometric Bimolecular Fluorescence Complementation (rBiFC)[33,36] in vivo. The in vitro approach offered quantitative information about possible multimer assemblies but was limited necessarily to work with the soluble N-termini. rBiFC analysis enabled a close comparison with the constructs expressed for the mbSUS studies and included internal controls for transformation and transgene loading. However, we did not expect the rBiFC studies to show puncta or a K^+ dependency, because VSD binding would 'cap' the interacting surfaces of any GORK channel assembly (Fig. 1a) and BiFC annealing renders a largely stable complex[36,37].

Gel filtration measurements (Supplemental Fig. 6) showed that the gVSD and $gVSD^{PNNP}$ N-termini eluted at apparent molecular weights near 26 kD, consistent with the formation of dimers as might be expected for intermolecular binding between adjacent channels (Fig. 1a). By contrast, both the kVSD and $gVSD^{NP}$ N-termini eluted as monomers near 13 kD. Confocal imaging (Supplemental Fig. 7) yielded similar results, showing a strong rBiFC signal in vivo on expressing GORK with gVSD and $gVSD^{PNNP}$ but not with kVSD or the non-interacting mutants $gVSD^{kNgS1\text{-}L4}$ and $gVSD^{NP}$. Thus, the most parsimonious explanation is that an alternation in charged surfaces along the N-termini enables interactions, zipper-like in register, with a complementarily charged surface between the VSD N-termini of GORK.

gVSD interactions affect GORK clustering and gating

To assess clustering, initially we introduced a selection of these mutations in the full-length channel tagged with GFP and expressed the constructs transiently in tobacco leaves for confocal image analysis. After mounting, the upper epidermis of leaf segments was removed and the lower epidermis and remaining mesophyll were superfused with 0.1 mM K^+ and then with 50 mM K^+ while imaging. Channel clustering was quantified in the epidermal cells by measuring GFP fluorescence along the cell periphery and calculating the relative standard deviation (RSD) from each of six or more independent experiments[20].

As before[20], a pronounced redistribution of the punctate GFP fluorescence of the leaf tissue expressing $GORK^{wt}$ when transferred from 0.1 mM to 50 mM K^+. We observed (Supplemental Fig. 8a) a similar K^+ dependence to clustering for $GORK^{PNNP}$, but each of the mutants $GORK^{kNgS1\text{-}L4}$, $GORK^{PN}$ and $GORK^{NP}$ gave little evidence of clustering, even in 0.1 mM K^+. Analysis of these experiments (Supplemental Fig. 8b) showed a significant decline in RSD with K^+ elevations for both $GORK^{wt}$ and $GORK^{PNNP}$; it also showed much reduced RSD values for $GORK^{kNgS1\text{-}L4}$, $GORK^{PN}$ and $GORK^{NP}$ that were unaffected by K^+ concentration, indicating that these mutant forms were dispersed around the cell periphery, their distribution independent of K^+ outside. Thus, we concluded that the mutations eliminating N-terminal binding also suppress GORK clustering.

GORK yields a current under voltage clamp that activates with positive-going voltage steps and decreasing K^+ outside; as a consequence, the steady-state current-voltage (IV) curve shifts positive-going with increasing external K^+ [16,20]. We observed much the same behavior when $GORK^{wt}$ was expressed in *Xenopus* oocytes (Supplemental Fig. 9a). Some differences in current amplitudes were evident between recordings, which may reflect true changes in maximum conductance or in expression and insertion of the channels in the plasma membrane as well as varations between oocytes[38]. However, the voltage dependencies of the currents were highly consistent. Expressing the same clustering-impaired constructs of $GORK^{kNgS1\text{-}L4}$, $GORK^{PN}$ and $GORK^{NP}$ (Supplemental Fig. 9b-d) led to negative-going shifts in the IV curves at each K^+ concentration relative to $GORK^{wt}$, but not when positively- and negatively-charged residues were exchanged with the $GORK^{PNNP}$ mutant (Supplemental Fig. 9e). In each case, channel expression was verified by immunoblot (Supplemental Fig. 15).

The ensemble current of a voltage-sensitive ion channel can be described by a Boltzmann function of the form

$$I = G_{max}\,(V-E_K)/(1+e^{\,\delta F(V-V_{1/2})/RT}) \qquad [1]$$

where G_{max} is the maximum ensemble conductance, V is the voltage, E_K is the equilibrium voltage for K^+, F is the Faraday constant, R is the universal gas constant, and T is the temperature. The parameters $V_{1/2}$ and δ define the midpoint voltage for gating and the sensitivity of the gate to a change in voltage, respectively. To quantify gating, we resolved the ensemble parameters G_{max}, $V_{1/2}$ and δ by joint, least-squares fitting to Eqn [1] of the steady-state K^+ currents across the K^+ concentrations (Supplemental Fig. 9a-e, *lines*)[33,34]. In each case, the analysis yielded visually satisfactory fittings with δ held in common and statistically significant shifts in $V_{1/2}$ with K^+ concentration. However, at any one K^+ concentration, $V_{1/2}$ values for $GORK^{kNgS1\text{-}L4}$, $GORK^{PN}$ and $GORK^{NP}$ were displaced by -19±2 to -46±5 mV, consistent with a

decrease in free energy for gating[39], ΔΔG, between -0.23 and -0.92 kcal/mol. Indeed, plotting $V_{1/2}$ as a function of K^+ concentration showed that each of the mutants affected in clustering also retained a dependence on K^+ outside; however, substantially higher K^+ concentrations were required to achieve a $V_{1/2}$ similar to the $GORK^{wt}$, indicating 3- to 8-fold decreases in the sensitivity to inhibition by K^+ (Supplemental Fig. 9f). In other words, mutating residues that promoted GORK clustering counterintuitively also appeared to reduce the free energy barrier for gating.

Manipulating GORK alters clustering and enhances K^+ currents in guard cells

To assess the consequences of the GORK mutations in vivo, we generated stable transformants of $GORK^{wt}$, $GORK^{kNgS1\text{-}L4}$, $GORK^{NP}$ and $GORK^{PNNP}$, again expressing the proteins with GFP tags. Lines were generated under control of the constitutive *pUB10* and guard cell-selective *pGC1* promoters[40,41] in the *gork* null mutant background of Arabidopsis. GORK transgene suppression had previously proven a difficulty[20]. We therefore analysed the T1 and, in some instances, the associated T2 generation of stable transformants driven by the *pGC1* promoter after selecting plants for growth on Basta and for GFP fluorescence. Individual transformed plants thus corresponded to independent transformants and were carried through the subsequent imaging, electrophysiology and gas exchange studies. We observed no systematic differences between transformants, and the results from the individual transformants are presented along with the pooled statistics. Plants complemented with $GORK^{wt}$ and $GORK^{PNNP}$ showed a peripheral clustering of the fluorescent marker in 0.1 mM K^+ that dispersed when K^+ outside was raised to 50 mM, much as observed in the wild type before[20]. However, plants complemented with the non-interacting GORK mutations exhibited a diffuse distribution of GFP fluorescence around the guard cell periphery, even in 0.1 mM K^+, that was unaffected by external K^+ (Fig. 3).

We recorded GORK currents under voltage clamp[42-44] from intact guard cells of the same plants and, as a control, from the *gork* null mutant background to confirm the lack of outward current (Supplemental Fig. 10). Recordings were carried out over an intermediate range of concentrations from 1 to 30 mM K^+ (Fig. 4a-e) to expose shifts in K^+-dependent gating[20]. As in the oocytes, guard cells of wild-type Arabidopsis and the $GORK^{wt}$- and $GORK^{PNNP}$-complemented *gork* mutant plants yielded currents that activated with positive-going voltage steps and IV curves that were displaced positive-going with increasing external K^+. Guard cells of the *gork* mutant complemented with the non-interacting GORK mutations showed similar currents and, as observed in the native GORK channel[18,19,31,45], G_{max} values that increased by 20-50% as K^+ was elevated from 1 to 30 mM outside; however, in this case the IV curves were shifted negative-going along the voltage axis at each K^+ concentration compared to the wild type current and the $GORK^{wt}$-complemented transformants. Mean steady-state currents were well-fitted using the Boltzmann function of Eqn [1] (Fig. 4a-e, *solid lines*) with a common value for δ but with significant displacements of $V_{1/2}$ for the non-interacting mutants. At 30 mM K^+, $V_{1/2}$ values for $GORK^{kNgS1\text{-}L4}$ and $GORK^{NP}$ were displaced by -28±4 and -17±3 mV (Fig. 4f) equivalent to ΔΔG values of -0.56 and -0.20 kcal/mol and a decrease in sensitivity to K^+ outside by factors of 7.4±0.9- and 4.5±0.4-fold, respectively, relative to the wild-type and $GORK^{wt}$ transformants. Thus, as in oocytes, each of the non-interacting mutants reduced the inhibition of channel activity by external K^+, whereas the $GORK^{PNNP}$ complementation rescued the wild-type characteristics.

GORK mutations impact on stomatal dynamics and gas exchange

Because the non-interacting mutations enhanced GORK current with voltage and external K^+ concentration, we anticipated that the effect should be evident as an acceleration in changes of stomatal conductance, g_s, following a closing stimulus. Incorporating a -30 mV shift of $V_{1/2}$ for GORK in simulations using the OnGuard3 platform[42,46] (Appendix 1) predicted an acceleration in g_s closing rates associated with a substantial increase in K^+ flux through GORK at voltages near and positive of E_K that are typical of guard cells during stomatal closing (Fig. 5a and Supplemental Figs. 11 and 12). Counterintuitively, they also predicted a small increase in the rate of opening, its dynamic range and steady-state g_s that could be ascribed to an inward conductance and K^+ uptake through GORK at voltages promoting stomatal opening introduced by the shift in $V_{1/2}$ (Fig. 4c,d and Supplemental Figs. 11).

To test these predictions, we recorded the gas exchange characteristics, again using the same plants employed for the analysis of clustering and channel gating (above). Experiments incorporated transitions to 200 μmol $m^{-2}s^{-1}$ photosynthetically-active radiation (PAR) from the dark and back again after preconditioning with 200 μmol $m^{-2}s^{-1}$ PAR. The results (Fig. 5a-c) confirmed a highly-significant accelerations of 1.4±0.1- and 1.6±0.2-fold for $GORK^{NP}$ and $GORK^{kNgS1\text{-}L4}$, respectively, in the rate of g_s decline on transit to dark. They also showed a small acceleration of opening and increases of 1.1±0.1 and 1.2±0.1-fold in steady-state g_s in the light, respectively.

The native GORK channel is expressed in vascular tissues and root hairs as well as guard cells and has been proposed to contribute broadly to K^+ homeostasis in the plant[16,47]. Our use of a guard cell-specific promoter to complement the *gork* null mutant suggested that any effects of the N-terminal modifications to GORK should arise from their impacts on guard cell K^+ flux. Nonetheless, to test for possible impacts on K^+ nutrition, we grew plants of the wild type, *gork* mutant, and *gork* mutant complemented with $GORK^{wt}$, $GORK^{kNgS1\text{-}L4}$, and $GORK^{NP}$ hydroponically with 20 μM and 2 mM K^+ after selection as before. These experiments (Supplemental Figure 13) showed a reduction in rosette area in all lines at 20 μM compared with 2 mM K^+, although the differences were small and not all were significant. No significant differences were observed in dry weight nor in growth between the *gork* mutant and any of the complemented lines. Total K^+ was generally reduced in each of the lines at 20 μM compared with 2 mM K^+ but, again, not all the differences were significant; no significant differences were observed between the wild type, $GORK^{wt}$, $GORK^{kNgS1\text{-}L4}$, and $GORK^{NP}$ complementations at any one concentration, suggesting that mutations affecting GORK gating had no substantive impact on K^+ homeostasis and each of the complementations was sufficient to restore normal K^+ content when compared with the *gork* null mutant.

One measure of plant performance is water use efficiency (WUE), often defined as the amount of dry mass produced per unit water transpired[2,48]. WUE is affected by light through the combined influence on carbon demand and associated transpiration. With the enhanced g_s and accelerated rates of stomatal movement we reasoned that the effects might translate to increases in WUE and biomass under fluctuating light. Light varies throughout the day in the natural environment, for example as clouds pass by. Photosynthesis generally tracks the energy input of light, but stomata are slower to respond to changes in light intensity, and this difference in kinetics can result in suboptimal assimilation rates when light intensity rises and to transpiration without corresponding assimilation when light intensity falls quickly[2]. Thus, we reasoned that accelerating stomatal closure by manipulating GORK gating might enhance WUE and carbon assimilation when integrated over a period of vegetative growth under fluctuating light.

We compared the growth of wild-type plants, the *gork* null mutant and the *gork* lines complemented with $GORK^{wt}$, $GORK^{kNgS1\text{-}L4}$ and $GORK^{NP}$ and $GORK^{PNNP}$ under control of the *pGC1* promoter. Plants of the *gork* mutant complemented with *pGC1*-driven constructs were selected as before. All lines were grown together under two light regimes, with plant exposed to a fixed daylight intensity of 140 μmol $m^{-2}s^{-1}$ PAR or to the same daylight period with varying light and the equivalent total fluence. For the fluctuating light regime, we stepped the light intensity between 10 and 220 μmol $m^{-2}s^{-1}$ with step intervals of 15 min, thus approximating the times normally required for stomatal closing and roughly half of that for opening. We also limited water availability under both regimes to impose a drought stress, maintaining soil moisture at 8±4% throughout the 5-week period of growth.

Rosette areas, fresh and dry weights of all plants were reduced under fluctuating light compared to the constant daylight conditions. Grown under the fluctuating light, however, the $GORK^{kNgS1\text{-}L4}$ and $GORK^{NP}$ transgenic plants showed greater rosette areas and dry weights compared to the wild-type control, $GORK^{wt}$ and $GORK^{PNNP}$ lines, and only marginally reduced when compared to plants grown under the fixed light regime (Fig. 5d-f). Total dry biomass of the $GORK^{kNgS1\text{-}L4}$ and $GORK^{NP}$ plants were enhanced 3.6±0.1- and 2.8±0.3-fold compared to the controls under varying light, which translated to a highly significant improvement in WUE of 2.3±0.1- and 1.8±0.2-fold, respectively, when compared to the wild-type plants grown under the fixed light regime (Fig. 5f). We confirmed that the increases in biomass were not the consequence of alterations in photosynthesis *per se*[49]: CO_2 assimilation under saturating light (600 μmol m^{-2} s^{-1}) was unaffected in any of the transgenic lines across the physiological range of internal CO_2 concentrations (Supplemental Fig. 14). Thus, complementing with GORK mutated to affect its gating, enhanced stomatal dynamics to improve water use efficiency and enhance carbon assimilation.

DISCUSSION

Ion channels are well known to assemble in clusters[31,50,51]. Channel clusters demarcate platforms for vesicle fusion in neurons[51,52] and they ally with cytoskeletal structures in muscle[51-53]. In plants, channel clusters arise with channel insertion and removal at the plasma membrane and respond to environmental signals[54,55]. The clustering of the Arabidopsis KAT1 K^+ channel, for example, is affected by the water-stress signal abscisic acid and its mobility in the membrane depends on direct binding to the vesicle-trafficking protein SYP121 at the plasma membrane[33,54,56]. GORK clustering diverges from these models. It is encoded entirely by the intrinsic structure of the channel protein itself and, like GORK channel gating, responds to K^+ outside [16,19,20].

Our findings now show that GORK clustering depends on binding between neighboring channels through their N-termini preceding the channel voltage sensor domains. It arises through conserved regions alternately of densities of positive and of negative charge that appear to interact, zipper-like in register, between the cytosolic N-termini and their complementary binding sites (Figs. 2, 3 and Supplemental Figs. 6-8). We find, too, that binding and clustering associate with, and impact on the voltage- and K^+-dependencies of GORK channel gating (Fig. 4 and Supplemental Fig. 9). Most important, we show that this feature can be harnessed to accelerate stomatal kinetics and improve WUE without a cost in carbon assimilation. Modelling predicted and experiments demonstrated that manipulating GORK gating to enhance guard cell K^+ flux accelerated stomatal kinetics as well as promoting stomatal conductance, g_s (Fig. 5). These findings offer a promising strategy, based on an ion channel native to the guard cell, for improving stomatal responsiveness and water use by the plant.

The cluster-gating paradox

For voltage-gated K^+ channels, in general, conformational changes of the voltage sensor and pore domain occur in 'lockstep', with the four VSDs of each channel working in concert to draw open the pore[30]. Thus, VSD dynamics affects opening and closing of the pore, just as K^+ occupation of the pore constrains VSD conformation. Details of the gating kinetics of GORK have yet to be established, but single-channel analyses are available for the near sequence-identical SKOR K^+ channel, which exhibits similar voltage- and K^+-dependencies[21,22]. The K^+ sensitivity of SKOR is mediated through K^+ occupation of the pore; it introduces a 'locked closed' state that precludes full relaxation of the channel to closure and, through its longer residence lifetime, constrains channel conformation and suppresses activity[22].

One plausible mechanistic model for GORK, then, is that clustering alters VSD mobility when fully relaxed to favor transition to the open state[18,45,57,58], and when sequestered in the 'locked closed' state, the VSD N-termini are unavailable for clustering interactions. In effect, interlacing the VSDs of adjacent channels together through their N-termini may create a cooperative network, or voltage 'sensory antenna', to favor channel conformations that reduce the energy barrier for channel opening at low- and submillimolar K^+ concentrations outside. This interpretation accords with the loss of the 'locked closed' state at low K^+ concentrations in the GORK homolog SKOR[22], and it is consistent with previous evidence from GORK that that Ba^{2+} occupation of the pore, like K^+, prevents GORK clustering[20]. Mutations affecting clustering also influenced the K^+-dependence of GORK gating, but the results proved counterintuitive: We anticipated that impairing clustering would suppress gating and displace the steady-state IV relations to the right along the voltage axis. Yet, paradoxically, mutations suppressing VSD interaction and clustering enhanced

channel activity as if the channels had nonetheless assembled in clusters (Figs. 4 and Supplemental Fig. 9).

How, then, might clustering integrate with gating? The simplest explanation is that the N-terminus must also suppress gating when not engaged in binding between VSDs to form clusters. In other words, the N-terminus may interact with a second site that inhibits gating when not bound with a neighboring channel, and both binding activities are affected by mutation of the N-terminus. We noted that the GORK VSD appears to harbor a secondary site with which the charged N-terminus of the full-length GORK channel interacts (see Fig. 1c)[59]. Thus, it is plausible that this site is available for interaction when the N-terminus is not bound with a neighboring channel and its binding amplifies the sensitivity of the gate to external K^+ (Fig. 6). Again, details of the crystal structure for GORK are lacking, but they are available for the Arabidopsis AKT1 K^+ channel[60] and the HCN1 K^+ channel of cardiac muscle[61]. Both AKT1 and HCN1 are members of the CNBD K^+ channel subfamily and incorporate VSDs with N-termini that intercallate within the same channel subunit between charged residues of the cyclic nucleotide-binding domain and the so-called 'C linker' hairpin positioned immediately below thei internal S4-S5 loop. In the HCN1 channel, binding of the N-terminus with the C linker enhances the cyclic nucleotide binding affinity as well as displacing the $V_{1/2}$ for channel gating[62] and in AKT1 this interaction is thought to alter the $V_{1/2}$ for channel gating[60]. We suggest that analogous interactions within the GORK channel subunit may determine the affinity for K^+ and the voltage dependence for GORK gating.

Shifting GORK gating enhances stomatal kinetics, water use and carbon gain

One immediate consequence for GORK of displacing $V_{1/2}$ negative-going is to enhance the capacity for K^+ flux at voltages near and positive of E_K (cf. Fig. 4 and Supplemental Fig. 11), voltages typical of the membrane during stomatal closure[6,57]. Thus, it is no surprise that the $GORK^{kNgS1\text{-}L4}$ and $GORK^{NP}$ mutants accelerated stomatal closure when compared to the wild-type and $GORK^{wt}$-complemented *gork* plants (Fig. 5). The observations clearly show that K^+ efflux is a rate-limiting factor determining net solute and turgor loss during closure. Displacing $V_{1/2}$ negative-going also explains the acceleration in stomatal opening (Fig. 5): as predicted by quantitative modelling (Supplemental Figs. 11 and 12), this displacement introduces a measurable current and inward-directed K^+ flux near and negative of E_K (Fig. 4c,d), voltages that normally promote solute uptake and stomatal opening[6,57]. In short, by manipulating GORK gating we enhance K^+ flux, both for stomatal opening and closing, introducing an additional conductance for K^+ to enhance stomatal kinetics, WUE and carbon assimilation (Figs. 5 and 6). This conductance compares favorably that of a synthetic, light-gated K^+ channel, which also enhanced stomatal kinetics, WUE and assimiation when expressed in guard cells[48].

Most important, our findings have strategic implications for crop improvement. The voltage- and K^+-dependencies of GORK are common among outward-rectifying K^+ channels of plants and contribute similarly to solute flux for stomatal movements[6,16,19]. These channels also share similar alternations in charge along their N-termini (Fig. 2a). Thus, the findings highlight potential molecular targets for gains in both WUE and photosynthetic carbon assimilation that should be achievable by engineering the corresponding ion channels native to the guard cells of crop plants. Indeed, by contrast with inclusion of a synthetic K^+ channel[48], altering the gating of the native GORK channel potentially circumvents the need for transgenic modification.

Much research to date has focused on enhancing WUE by reducing stomatal densities, an approach that decreases transpiration but can also reduce CO_2 availability for photosynthesis and slow plant growth[2,63,64]. Some studies have shown that altering the populations of ion pumps and channels will affect stomatal conductance and photosynthesis, but commonly at the expense either of WUE or of carbon assimilation[42,43,65-67]. Indeed, a mechanistic analysis of stomata[65] has called into question strategies that focus on manipulating transporter populations alone as a means to improving stomatal performance; the analysis suggests that targeting the control of transport, including the gating mechanics of ion channels, is more likely to be effective.

Our findings now demonstrate the efficacy of altering the gating in an ion channel native to the guard cell. By introducing mutations that affect GORK channel clustering, we have altered the voltage- and K^+-dependencies for K^+ flux, enhancing guard cell membrane transport and accelerating stomatal movements. These findings underscore the gains possible by 'tuning' the gating of channels native to the plant to improve WUE and carbon assimilation, thus circumventing the often conflicting demands in conserving water while ensuring photosynthetic assimilation for growth.

MATERIAL AND METHODS

Molecular biology, split-ubiquitin assays and biochemistry

All constructs were generated using Gateway-compatible destination vectors described previously after entry vector sequencing[36,40,68]. The Supplemental Methods, Fig. 2 and Supplemental Figs. 2-4 summarize the construct and cloning strategies. Primer sequences are listed in Supplemental Tables 1-3. Split-ubiquitin assays were carried out using C-terminal X-Cub-PLV bait fusions in THY.AP4, and the NubG-Y prey fusions or NubI and NubG as positive and negative controls, respectively, in THY.AP5[69]. Serial dilutions of yeast were dropped at 10 µl per spot onto SCM_{-LTUM} plates to verify mating and on the same medium without alanine and histidine ($SCM_{-LTUMAH}$) without and with increasing methionine concentrations to test for interaction. Expression was verified by immunoblot (see Supplemental Figure 15).

Recombinant peptide synthesis and gel filtration assays for N-terminal multimers were carried out as before[70] and are described in the Supplemental Methods. Gel filtration eluates were assessed against molecular weight standards and band intensities quantified against known molar quantities of the same proteins.

Plant growth, transformation and whole-plant physiology

Tobacco (*Nicotiana tabacum*) were grown and leaves transformed by *Agrobacterium* infiltration[71]. Arabidopsis (*Arabidopsis thaliana*) wild-type (Col0), the *gork* null mutant[16,20] and its complementation lines were sterilized and grown at 22:18 ^{o}C and 9:15 h light:dark cycles. For hydroponic growth analysis, seedlings were selected after 2-wk growth on Basta and transferred to defined liquid media with 20 µM, and 2 mM K^+ and were maintained with solution exchange for 3 wk before harvest[72]. The media composition is included in Supplemental Methods. The characteristics of the *gork* mutant background and its phenotype are described elsewhere[16,20].

Gas exchange measurements and growth experiments were carried out using LICOR 6800 gas exchange systems (Lincoln, USA) as described previously[42,43,46]. Soil water content was monitored using a ML3 moisture sensor (DeltaT Devices, Cambridge UK) and plants watered at 1- to 3-d intervals to maintain 8±4% soil water content.

Confocal microscopy

Transformed tobacco and Arabidopsis leaves were imaged on a Leica SP8 SMD confocal microscope equipped with 20x/0.85 NA dry and 40x/1.3 NA oil lenses and hybrid GaAs detectors (Leica, Wetzlar, Germany). Fluorescence was excited with the 488, 514 and 552 nm laser lines. GFP, YFP and RFP fluorescence, the latter two for rBiFC, were collected across 495-550, 520-570, and 580-630 nm, respectively. Chloroplast autofluorescence was excited with 488 nm light and collected across 630-690 nm. Laser intensities and detector gains were standardized between sets of experiments for quantative analysis. Fluorescence signals were analysed using ImageJ v.1.53o[73].

Electrophysiology

K^+ channels expressed in *Xenopus* oocytes were measured using a standard protocols and a two-electrode voltage clamp[20,32,39]. cRNAs were injected at 1 ng/oocyte. Recordings were carried out 48-72 h after injection and oocytes were collected and analyzed for protein expression. Oocytes were superfused with 1, 10,

30 and 60 mM K^+ in modified ND96 buffer with 1.8 mM $MgCl_2$, 1.8 mM $CaCl_2$ and 10 mM HEPES-NaOH, pH 7.2 adjusted for osmotic balance[32,69]. All recordings were carried out using Henry's EP suite (v. 3.5.5.5, Y-Science, Glasgow, UK).

Currents from intact guard cells in epidermal peels were recorded using double-barrelled microelectrodes and Henry's EP suite. Guard cells were superfused with 1, 10, and 30 mM KCl in 5 mM Ca^{2+}-MES, pH 6.1 ($[Ca^{2+}]$ = 1 mM)[42,43]. Voltage was clamped in cycles from holding voltages at least -50 mV from E_K with postive-going steps for outward-rectifying currents. Voltage was clamped in cycles from a holding voltage of -100 mV with negative-going steps for inward-rectifying currents. Currents were analyzed using Henry's EP suite (Y-Science, Glasgow) and SigmaPlot 11.2 (Systat Software, Inc., USA) as described previously[20,46,74,75], and steady-state currents were fitted by joint, non-linear least-squares using the Boltzmann function of Eqn [1][20,33,46].

OnGuard modelling and statistics

Quantitative modelling using OnGuard3[42,46,76-78] is described in Supplemental Methods and Appendix 1. All other results are reported as means ±SE of *n* independent experiments. Significance was determined by Analysis of Variance (ANOVA), as appropriate with post-hoc analysis (Student-Newman-Keuls, Holm-Sidek and Tukey), and is indicated at $P<0.05$ unless otherwise stated.

Acknowledgements: This work was supported by BBSRC grants BB/L001276/1, BB/L019205/1, BB/M001601/1, and BB/ T013508/1 to MRB, by a Royal Thai PhD studentship to WH, a University of Glasgow Doctoral Training Studentship to WC, an Lord Kelvin-Adam Smith Doctoral Fellowship to FALS-A, and BBSRC grant BB/R019894/1 to AA. We thank Naomi Donald for support in mbSUS assays and Amparo Ruiz-Pardo for help in plant maintenance.

Author contributions: MRB conceived the work and developed the strategies for analysis with BZ, JA and AH; WH, WC and BZ carried out and analyzed the mbSUS assays; WH carried out oocyte electrophyiology and, with JA, MK and MRB, the confocal, gas exchange and the growth studies; MK carried out the guard cell electrophysiology and analysed the results with MRB; SW expressed and purified the channel N-termini and carried out the gel filtration studies; MP and AA undertook the hydroponic growth studies; MRB carried out the modelling with AH, JA, WH, FALS-A and MK; MRB wrote the manuscript and all authors edited and approved the manuscript.

Competing interests: The authors declare no competing interests.

Data and code availability: Data generated and analysed during this study are included in the article, its supplementary information files, and are also available on reasonable request to the corresponding author. The OnGuard3 platform and the model parameter sets are freely available to academic users and may be downloaded from www.psrg.org.uk

Supplemental Material:

Supplemental Methods
Supplemental Table 1. **Forward and Reverse PCR primer pairs used in preparing the products listed**
Supplemental Table 2. **PCR primers**
Supplemental Table 3. **PCR primers for GORK N-terminal purification**
Supplemental Appendix 1. **OnGuard3 model parameters for wild-type and modified GORK (mGORK) Arabidopsis**

References

1 Hetherington, A. M. & Woodward, F. I. The role of stomata in sensing and driving environmental change. *Nature* **424**, 901-908 (2003).

2 Lawson, T. & Blatt, M. R. Stomatal Size, Speed, and Responsiveness Impact on Photosynthesis and Water Use Efficiency. *Plant physiology* **164**, 1556-1570 (2014).

3 Beljaars, A. C. M., Viterbo, P., Miller, M. J. & Betts, A. K. The anomalous rainfall over the United States during July 1993: Sensitivity to land surface parameterization and soil moisture. *Mon. Weather Rev.* **124**, 362-383, doi:10.1175/1520-0493(1996)124<0362:tarotu>2.0.co;2 (1996).

4 Berry, J. A., Beerling, D. J. & Franks, P. J. Stomata: key players in the earth system, past and present. *Current Opinion In Plant Biology* **13**, 233-240 (2010).

5 Unesco. *Water for a Sustainable World -- UN World Water Development Report*. Vol. 1 (UNESCO, 2015).

6 Jezek, M. & Blatt, M. R. The Membrane Transport System of the Guard Cell and Its Integration for Stomatal Dynamics. *Plant physiology* **174**, 487-519, doi:10.1104/pp.16.01949 (2017).

7 Assmann, S. M. & Jegla, T. Guard cell sensory systems: recent insights on stomatal responses to light, abscisic acid, and CO2. *Current Opinion in Plant Biology* **33**, 157-167, doi:10.1016/j.pbi.2016.07.003 (2016).

8 Nakamura, R. L. *et al.* Expression of an Arabidopsis potassium channel gene in guard cells. *Plant physiology* **109**, 371-374 (1995).

9 Pilot, G., Gaymard, F., Mouline, K., Cherel, I. & Sentenac, H. Regulated expression of Arabidopsis Shaker K + channel genes involved in K + uptake and distribution in the plant. *Plant Molecular Biology* **51**, 773-787 (2003).

10 Lebaudy, A. *et al.* Plant adaptation to fluctuating environment and biomass production are strongly dependent on guard cell potassium channels. *Proceedings Of The National Academy Of Sciences Of The United States Of America* **105**, 5271-5276 (2008).

11 Pilot, G. *et al.* Guard cell inward K + channel activity in Arabidopsis involves expression of the twin channel subunits KAT1 and KAT2. *Journal Of Biological Chemistry* **276**, 3215-3221 (2001).

12 Clint, G. M. & Blatt, M. R. Mechanisms of fusicoccin action: evidence for concerted modulations of secondary K^+ transport in a higher-plant cell. *Planta* **178**, 495-508 (1989).

13 Blatt, M. R. & Clint, G. M. Mechanisms of fusicoccin action kinetic modification and inactivation of potassium channels in guard cells. *Planta* **178**, 509-523 (1989).

14 Maathuis, F. J. M. & Sanders, D. Mechanism of high-affinity potassium uptake in roots of Arabidopsis thaliana *Proceedings Of The National Academy Of Sciences Of The United States Of America* **91**, 9272-9276 (1994).

15 Very, A.-A. *et al.* Molecular biology of K^+ transport across the plant cell membrane: What do we learn from comparison between plant species? *Journal of Plant Physiology* **171**, 748-769, doi:10.1016/j.jplph.2014.01.011 (2014).

16 Hosy, E. *et al.* The Arabidopsis outward K^+ channel GORK is involved in regulation of stomatal movements and plant transpiration. *Proceedings Of The National Academy Of Sciences Of The United States Of America* **100**, 5549-5554 (2003).

17 Ache, P. *et al.* GORK, a delayed outward rectifier expressed in guard cells of Arabidopsis thaliana, is a K^+ -selective, K^+ -sensing ion channel. *FEBS Letters* **486**, 93-98 (2000).
18 Blatt, M. R. Potassium-dependent bipolar gating of potassium channels in guard cells. *Journal Of Membrane Biology* **102**, 235-246 (1988).
19 Blatt, M. R. & Gradmann, D. K^+ -sensitive gating of the K^+ outward rectifier in Vicia guard cells. *Journal Of Membrane Biology* **158**, 241-256 (1997).
20 Eisenach, C., Papanatsiou, M., Hillert, E. K. & Blatt, M. R. Clustering of the K^+ channel GORK of Arabidopsis parallels its gating by extracellular K^+ *Plant Journal* **78**, 203-214 (2014).
21 Gaymard, F. *et al.* Identification and disruption of a plant shaker-like outward channel involved in K + release into the xylem sap. *Cell* **94**, 647-655 (1998).
22 Johansson, I. *et al.* External K + modulates the activity of the Arabidopsis potassium channel SKOR via an unusual mechanism. *Plant Journal* **46**, 269-281 (2006).
23 Riedelsberger, J. *et al.* Distributed Structures Underlie Gating Differences between the K_{in} Channel KAT1 and the K_{out} Channel SKOR. *Molecular Plant* **3**, 236-245 (2010).
24 Gajdanowicz, P. *et al.* Distributed structures determine K^+ and voltage dependent gating of the K_{in} channel KAT1 and the K_{out} channel SKOR. *New Phytologist* **182**, 380-391 (2009).
25 Jegla, T., Busey, G. & Assmann, S. M. Evolution and Structural Characteristics of Plant Voltage-Gated K+ Channels. *Plant Cell* **30**, 2898-2909, doi:10.1105/tpc.18.00523 (2018).
26 Pozdnyakov, I., Safonov, P. & Skarlato, S. Diversity of voltage-gated potassium channels and cyclic nucleotide-binding domain-containing channels in eukaryotes. *Scientific Reports* **10**, 13, doi:10.1038/s41598-020-74971-4 (2020).
27 Dreyer, I. & Blatt, M. R. What makes a gate? The ins and outs of Kv-like K^+ channels in plants. *Trends In Plant Science* **14**, 383-390 (2009).
28 Very, A. A. & Sentenac, H. Cation channels in the Arabidopsis plasma membrane. *Trends In Plant Science* **7**, 168-175 (2002).
29 Yellen, G. The voltage-gated potassium channels and their relatives. *Nature* **419**, 35-42 (2002).
30 Palovcak, E., Delemotte, L., Klein, M. L. & Carnevale, V. Evolutionary imprint of activation: The design principles of VSDs. *Journal of General Physiology* **143**, 145-156 (2014).
31 Lefoulon, C. The bare necessities of plant K+ channel regulation. *Plant physiology* **187**, 2092-2109, doi:10.1093/plphys/kiab266 (2021).
32 Lefoulon, C. *et al.* Voltage-sensor transitions of the inward-rectifying K^+ channel KAT1 indicate a closed-to-open latching mechanism that is biased by hydration around the S4 alpha-helix. *Plant physiology* **166**, 960-975, doi:0.1104/pp.114.244319 (2014).
33 Grefen, C. *et al.* A vesicle-trafficking protein commandeers Kv channel voltage sensors for voltage-dependent secretion. *Nature Plants* **1**, 15108-15119, doi:DOI: 10.1038/NPLANTS.2015.108 (2015).
34 Honsbein, A. *et al.* A Tripartite SNARE-K^+ Channel Complex Mediates in Channel-Dependent K^+ Nutrition in Arabidopsis *Plant Cell* **21**, 2859-2877 (2009).

35 Grefen, C., Obrdlik, P. & Harter, K. The determination of protein-protein interactions byt the mating-based split-ubiquitin system (mbSUS). *Methods in Molecular Biology* **479**, 1-17 (2009).
36 Grefen, C. & Blatt, M. R. A 2in1 cloning system enables ratiometric bimolecular fluorescence complementation (rBiFC). *Biotechniques* **53**, 311-314 (2012).
37 Fricker, M. D., Runions, J. & Moore, I. Quantitative fluorescence microscopy: from art to science. *Ann.Rev.Plant Biology* **57**, 79-107 (2006).
38 Gould, G. W. *Membrane Protein Expression Systems*. Vol. 1 (Portland Press, 1994).
39 Lefoulon, C., Waghmare, S., Karnik, R. & Blatt, M. R. Gating control and K+ uptake by the KAT1 K+ channel leaveraged through membrane anchoring of the trafficking protein SYP121. *Plant Cell and Environment* **41**, 2668-2677, doi:10.1111/pce.13392 (2018).
40 Grefen, C. *et al.* A ubiquitin-10 promoter-based vector set for fluorescent protein tagging facilitates temporal stability and native protein distribution in transient and stable expression studies. *Plant Journal* **64**, 355-365 (2010).
41 Yang, Y. Z., Costa, A., Leonhardt, N., Siegel, R. S. & Schroeder, J. I. Isolation of a strong Arabidopsis guard cell promoter and its potential as a research tool. *Plant Methods* **4**, 4-6, doi:10.1186/1746-4811-4-6 (2008).
42 Wang, Y. *et al.* Unexpected Connections between Humidity and Ion Transport Discovered using a Model to Bridge Guard Cell-to-Leaf Scales. *Plant Cell* **29**, 2921-2139, doi:10.1105/tpc.17.00694 (2017).
43 Wang, Y. *et al.* Systems dynamic modelling of a guard cell Cl^- channel mutant uncovers an emergent homeostatic network regulating stomatal transpiration. *Plant physiology* **160**, 1956-1972 (2012).
44 Eisenach, C., Chen, Z. H., Grefen, C. & Blatt, M. R. The trafficking protein SYP121 of Arabidopsis connects programmed stomatal closure and K^+ channel acivity with vegetative growth. *Plant Journal* **69**, 241-251 (2012).
45 Blatt, M. R. K^+ channels of stomatal guard cells: characteristics of the inward rectifier and its control by pH. *Journal of General Physiology* **99**, 615-644 (1992).
46 Jezek, M. *et al.* Guard cell endomembrane Ca^{2+}-ATPases underpin a 'carbon memory' of photosynthetic assimilation that impacts on water use efficiency. *Nature Plants* **7**, 1301-1307, doi:https://doi.org/10.1038/s41477-021-00966-2 (2021).
47 Becker, D. *et al.* Regulation of the ABA-sensitive Arabidopsis potassium channel gene GORK in response to water stress. *Febs Letters* **554**, 119-126, doi:10.1016/s0014-5793(03)01118-9 (2003).
48 Papanatsiou, M. *et al.* Optogenetic manipulation of stomatal kinetics improves carbon assimilation and water use efficiency. *Science* **363**, 1456-1459 (2019).
49 Sharkey, T. D., Bernacchi, C. J., Farquhar, G. D. & Singsaas, E. L. Fitting photosynthetic carbon dioxide response curves for C-3 leaves. *Plant Cell and Environment* **30**, 1035-1040, doi:10.1111/j.1365-3040.2007.01710.x (2007).
50 Tester, M. Plant ion channels: whole-cell and single-channel studies. *New Phytologist* **114**, 305-340 (1990).
51 Lai, H. C. & Jan, L. Y. The distribution and targeting of neuronal voltage-gated ion channels. *Nature Reviews Neuroscience* **7**, 548-562 (2006).
52 Deutsch, E. *et al.* Kv2.1 cell surface clusters are insertion platforms for ion channel delivery to the plasma membrane. *Molecular Biology of the Cell* **23**, 2917-2929, doi:10.1091/mbc.E12-01-0047 (2012).

53 Tamkun, M. M., O'Connell, K. M. S. & Rolig, A. S. A cytoskeletal-based perimeter fence selectively corrals a sub-population of cell surface Kv2.1 channels. *Journal of Cell Science* **120**, 2413-2423 (2007).
54 Sutter, J. U., Campanoni, P., Tyrrell, M. & Blatt, M. R. Selective mobility and sensitivity to SNAREs is exhibited by the Arabidopsis KAT1 K^+ channel at the plasma membrane. *Plant Cell* **18**, 935-954 (2006).
55 Sutter, J. U. *et al.* Abscisic acid triggers the endocytosis of the Arabidopsis KAT1 K^+ channel and its recycling to the plasma membrane. *Current Biology* **17**, 1396-1402 (2007).
56 Karnik, R. *et al.* Commandeering Channel Voltage Sensors for Secretion, Cell Turgor, and Volume Control. *Trends In Plant Science* **11**, 81-95 (2017).
57 Thiel, G., MacRobbie, E. A. C. & Blatt, M. R. Membrane transport in stomatal guard cells: the importance of voltage control. *Journal Of Membrane Biology* **126**, 1-18 (1992).
58 Blatt, M. R. Potassium channel currents in intact stomatal guard cells: rapid enhancement by abscisic acid. *Planta* **180**, 445-455 (1990).
59 Horaruang, W. *The Mechanism of GORK K^+ channel gating and clustering* PhD thesis, University of Glasgow, (2019).
60 Dickinson, M. S., Pourmal, S., Gupta, M., Bi, M. & Stroud, R. M. Symmetry Reduction in a Hyperpolarization-Activated Homotetrameric Ion Channel. *Biochemistry* **in press**, doi:10.1021/acs.biochem.1c00654 (2022).
61 Lee, C.-H. & MacKinnon, R. Structures of the Human HCN1 Hyperpolarization-Activated Channel. *Cell* **168**, 111-+, doi:10.1016/j.cell.2016.12.023 (2017).
62 Porro, A. *et al.* The HCN domain couples voltage gating and cAMP response in hyperpolarization-activated cyclic nucleotide-gated channels. *Elife* **8**, e49672, doi:10.7554/eLife.49672 (2019).
63 Doheny-Adams, T., Hunt, L., Franks, P. J., Beerling, D. J. & Gray, J. E. Genetic manipulation of stomatal density influences stomatal size, plant growth and tolerance to restricted water supply across a growth carbon dioxide gradient. *Philosophical Transactions of the Royal Society B-Biological Sciences* **367**, 547-555, doi:10.1098/rstb.2011.0272 (2012).
64 Masle, J., Gilmore, S. R. & Farquhar, G. D. The ERECTA gene regulates plant transpiration efficiency in Arabidopsis *Nature* **436**, 866-870 (2005).
65 Wang, Y., Hills, A. & Blatt, M. R. Systems analysis of guard cell membrane transport for enhanced stomatal dynamics and water use efficiency. *Plant physiology* **164**, 1593-1599 (2014).
66 Kusumi, K., Hirotsuka, S., Kumamaru, T. & Iba, K. Increased leaf photosynthesis caused by elevated stomatal conductance in a rice mutant deficient in SLAC1, a guard cell anion channel protein. *Journal of Experimental Botany* **63**, 5635-5644, doi:10.1093/jxb/ers216 (2012).
67 Wang, Y. *et al.* Overexpression of plasma membrane H^+ -ATPase in guard cells promotes light-induced stomatal opening and enhances plant growth. *Proc.Nat.Acad.Sci.USA* **111**, 533-538 (2014).
68 Hecker, A. *et al.* Binary 2in1 vectors improve in planta (co-) localisation and dynamic protein interaction studies. *Plant physiology* **168**, 776-787, doi:10.1104/pp.15.00533 (2015).
69 Grefen, C. *et al.* A Novel Motif Essential for SNARE Interaction with the K^+ Channel KC1 and Channel Gating in Arabidopsis *Plant Cell* **22**, 3076-3092 (2010).

70 Waghmare, S. *et al.* K+ Channel-SEC11 Binding Exchange Regulates SNARE Assembly for Secretory Traffic. *Plant physiology* **181**, 1096-1113, doi:10.1104/pp.19.00919 (2019).
71 Tyrrell, M. *et al.* Selective targeting of plasma membrane and tonoplast traffic by inhibitory (dominant-negative) SNARE fragments. *Plant Journal* **51**, 1099-1115 (2007).
72 Sani, E., Herzyk, P., Perrella, G., Colot, V. & Amtmann, A. Hyperosmotic priming of Arabidopsis seedlings establishes a long-term somatic memory accompanied by specific changes of the epigenome. *Genome Biology* **14**, doi:10.1186/gb-2013-14-6-r59 (2013).
73 Rasband, W. S. & Bright, D. S. NIH IMAGE - A public domain image-processing program for the Macintosh. *Microbeam Analysis* **4**, 137-149 (1995).
74 Chen, Z. H., Hills, A., Lim, C. K. & Blatt, M. R. Dynamic regulation of guard cell anion channels by cytosolic free Ca^{2+} concentration and protein phosphorylation. *Plant Journal* **61**, 816-825 (2010).
75 Blatt, M. R. Electrical characteristics of stomatal guard cells: the contribution of ATP-dependent, "electrogenic" transport revealed by current-voltage and difference-current-voltage analysis. *Journal Of Membrane Biology* **98**, 257-274 (1987).
76 Hills, A., Chen, Z. H., Amtmann, A., Blatt, M. R. & Lew, V. L. OnGuard, a Computational Platform for Quantitative Kinetic Modeling of Guard Cell Physiology. *Plant physiology* **159**, 1026-1042 (2012).
77 Chen, Z. H. *et al.* Systems Dynamic Modeling of the Stomatal Guard Cell Predicts Emergent Behaviors in Transport, Signaling, and Volume Control. *Plant physiology* **159**, 1235-1251 (2012).
78 Jezek, M., Hills, A., Blatt, M. R. & Lew, V. L. A constraint-relaxation-recovery mechanism for stomatal dynamics. *Plant, Cell & Environment* **42**, 2399-2410, doi:10.1111/pce.13568 (2019).
79 Karnik, R. *et al.* Arabidopsis Sec1/Munc18 Protein SEC11 Is a Competitive and Dynamic Modulator of SNARE Binding and SYP121-Dependent Vesicle Traffic. *Plant Cell* **25**, 1368-1382 (2013).
80 Clough, S. J. & Bent, A. F. Floral dip: a simplified method for Agrobacterium-mediated transformation of Arabidopsis thaliana. *Plant Journal* **16**, 735-743 (1998).

Figure legends

Figure 1. **GORK K^+ channels interact through the cytosolic N-termini of the voltage sensor domains**
(a) Schematic of Kv channel subunit structure (*above*) with the six, transmembrane α-helices (S1-S6), intervening loops (L1-L4) and chimera exchange points (---, see also Supplemental Figure 2) indicated. Four homologous subunits assemble around a central pore to give a functional channel with the voltage-sensor domains (VSDs) forming an outer ring within the plane of the membrane (①). Neighboring channels may come together bridged by interactions between VSDs (②), but interactions between subunits will also occur between individual subunits within the channel assembly (①). Exploring interactions between VSDs therefore requires to isolate one VSD component (③).
(b) Selective binding occurs between GORK and the GORK VSD (gVSD) but is not evident with either KAT1 or its VSD (kVSD). Cartoons (left) indicate the bait and prey structures. One of three independent experiments, all yielding similar results. Yeast mating-based split-ubiquitin assay for interaction of the Nub-X channel and VSD fusions, including controls ([-], NubG; [+], NubI), with the GORK-Cub bait fusion. Yeast diploids dropped at 1.0 and 0.1 OD_{600} spotted (*left to right*) on complete synthetic medium without Trp, Leu, Ura and Met (CSM_{-LTUM}) to verify mating, on CSM without Trp, Leu, Ura, Ade, His and Met ($CSM_{-LTUMAH}$) to verify adenine- and histidine-independent growth, and with Met additions to suppress bait expression. Immunoblots are included in Supplemental Fig. 15.
(c) Chimeras of the GORK VSD (gVSD) and KAT1 VSD (kVSD) interact with the full-length GORK channel provided the VSD prey includes the gVSD N-terminus. Cartoons (*left*) indicate the bait and prey structures (see also Supplemental Fig. 2). One of three independent experiments, all yielding similar results. Yeast mating-based split-ubiquitin assay for interaction of the Nub-X VSD and VSD chimera fusions, including controls ([-], NubG; [+], NubI), with the GORK-Cub bait fusion as in (b). Immunoblots are included in Supplemental Fig. 15.

Figure 2. **Alternation of charges defines GORK VSD interactions**
Mutation of the GORK VSD N-terminus supports interaction provided the alternation of charges is retained.
(a) Alignment of the N-terminal cytosolic domains GORK homologs highlights an alternation of positive and negative charged regions. Sequences (NCBI identifiers) from *Arabidopsis thaliana* GORK (CAC17380.1) and SKOR (NC_003074.8), *Brassica napus* (XP_013656069.1), Arabidopsis relative *Tarenaya hassleriana* (XP_010553885.1), oil palm *Elaeis guineensis* (XP_010905454.2), pepper *Capsicum annuum* (KAF3658364.1), wheat *Triticum aestivum* (XP_044442180.1), rice *Oriza sativa* (XP_015644419.1), *Sellaginella magellanicum* (KAH9569187.1), *Physcomitrella patens* (XP_024370995.1), *Chlamydomonas eustigma* (GAX83177.1) and, for comparison, *Arabidopsis thanliana* KAT1 (NC_003076.8) and AKT1 (NC_003071.7). Charged residues (positive, *blue*; negative, *yellow*) are highlighted. Note the alternation in densities between negatively- and positively-charged residues in the angiosperm GORK and GORK-like channels.
(b) Alignment of the GORK and KAT1 N-termini. Negative and positive charged residues were exchanged in $gVSD^{PN}$ and $gVSD^{NP}$, respectively, and are substituted with Ala in $gVSD^{A}$. His residues were included as these carry a substantial positive charge at neutral pH. All charged residues were exchanged in $gVSD^{PNNP}$.

(c) One of three independent experiments, all yielding similar results testing the residue mutants in (b) for interaction with the full-length GORK channel here cross-referenced by color coding (*left*). Yeast mating-based split-ubiquitin assay for interaction of the Nub-X VSD fusions, including controls ([-], NubG; [+], NubI), with the GORK-Cub bait fusion. Yeast diploids dropped at 1.0 and 0.1 OD_{600} spotted (*left to right*) on complete synthetic medium without Trp, Leu, Ura and Met (CSM_{-LTUM}) to verify mating, on CSM without Trp, Leu, Ura, Ade, His and Met ($CSM_{-LTUMAH}$) to verify adenine- and histidine-independent growth, and with Met additions to suppress bait expression. Immunoblots are included in Supplemental Fig. 15.

Figure 3. **Non-interacting channel mutations suppress GORK clustering when stably expressed in Arabidopsis**
(a) Confocal analysis of GFP channel fusions (GFP), chlorophyll fluorescence (Chlpst), and corresponding brightfield (Bright) images from *gork* Arabidopsis leaf epidermis transformed with wild-type GORK-GFP ($GORK^{wt}$), GFP fusions of the non-interacting mutations $GORK^{kN\text{-}gS1\text{-}L4}$ and $GORK^{NP}$, and the interacting $GORK^{PNNP}$ mutant under control of the guard cell *pGC1* promoter. Representative image sets from leaves infiltrated[20] with 0.1 mM and subsequently with 50 mM K^+. Scale bar, 10 µm. Note the expanded views (GFP expanded, *right*) of the boxed regions in each image (*left*) with arrows indicating the puncta visible at the periphery in 0.1 mM K^+ for the $GORK^{wt}$- and $GORK^{PNNP}$-complemented lines.
(b) Relative standard deviation (RSD) of GFP distributions. RSD calculated from the GFP fluorescence measured along a 1 µm-wide line traced around the periphery of 10 guard cells selected at random in n>6 independent experiments with each construct. Data are means ±SE for 0.1 (●) and 50 mM (❍) K^+ with means from individual experiments indicated by the smaller grey symbols, each experiment corresponding to an independent transformant. Note the logarithmic scale. Significant differences at P<0.02 are indicated by lettering.

Figure 4. **Non-interacting GORK channel mutations express functional K^+ channels with displaced midpoint voltages**
Representative current traces and steady-state current-voltage (IV) curves recorded under voltage clamp from guard cells of wild-type Arabidopsis (a) and guard cells of the *gork* mutant background complemented with GFP fusions of wild-type GORK ($GORK^{wt}$, b), the non-interacting mutations $GORK^{kN\text{-}gS1\text{-}L4}$ (c) and $GORK^{NP}$ (d), and the interacting $GORK^{PNNP}$ mutation (e) under control of the guard cell *pGC1* promoter. IV curves are means ±SE of n>6 independent experiments comprising measurements from individual guard cells superfused successively with 1 (filled circles), 10 (grey circles), and 30 mM (open circles) K^+ outside, cross-referenced by symbol. Each experiment with the *gork* mutant complementations corresponds to an independent transformant, with data sets for the $GORK^{wt}$, $GORK^{kNgS1\text{-}L4}$ and $GORK^{NP}$ included as the smaller grey symbols in (f). Scale bar: horizontal, 1 s; vertical, 100 µA cm^{-2}. Lines are joint, least-squares fittings to Eqn [1]. Fittings yielded a common δ of 1.82±0.04. Means ±SE for $V_{1/2}$ from these fittings, summarized in (f), show a significant negative shift for each of the non-interacting mutant channels. Significant differences at P<0.05 across all K^+ concentrations are indicated by letters (*right*). Note that changing [K^+] outside had only a modest effect on current amplitude, as expected, because K^+ carrying GORK current comes from inside the cell.

Figure 5. **Non-interacting GORK channel mutations accelerate stomatal closure and enhance water use efficiency**

Experimental data incorporate measurements from the same plants as in Figs. 3 and 4 driven by the guard cell-specific promoter *pGC1*. Significant differences (P<0.02) are indicated by letters below in each case.

(a) Stomatal conductance (g_s) responses to a 100 min light step of 200 μmol $m^{-2}s^{-1}$ PAR following a 1-h dark period (*above*). Simulation outputs (*left*) are for wild-type (wt), GORK with a -30 mV displacement in $V_{1/2}$ (mGORK; see Fig. 4 and Supplemental Figs. 11 and 12) and for the *gork* nul mutant. Experimental data (*right*) are means ±SE of n>5 independent experiments on wild-type (wt), the nul mutant background (*gork*), and the same background expressing the $GORK^{NP}$ mutation.

(b) Closing rate constants for the simulations (diamonds) and experimental measurements including those in (a). Rate constants were determined from fittings to a first order exponential function and are shown for each measurement (grey circles), corresponding to independent transformants, and as means ±SE of these data (black circles).

(c) Opening halftimes for the simulations (diamonds) and experimental measurements including those in (a). Halftimes are shown for each measurement (grey circles), corresponding to independent transformants, and as means ±SE of these data (black circles).

(d) Representative wild-type, *gork* mutant and $GORK^{wt}$, $GORK^{kN\text{-}gS1\text{-}L4}$, $GORK^{NP}$ and $GORK^{PNNP}$ complemented *gork* mutant plants after 5 wk growth under fixed and varying light regimes (see Methods).

(e,f) Rosette areas (e), dry biomass and water use efficiencies (f) for all plants, including the plants shown in (a-d). Small circles are individual plants (open, fixed light; filled, varying light), corresponding to independent transformants; large circles (open, fixed light; filled, varying light) are means ±SE for each set of plants (wild-type n=11 plants; mutant and complemented n>8 plants). Note the separate WUE scales for plants grown under fixed and varying light.

Figure 6. **A mechanism coupling GORK clustering and gating through a binding exchange of the VSD N-terminus**

We start with the assumption that elevating K^+ outside facilitates transition from the open channel to a 'locked closed' state, similar to the SKOR K^+ channel (*left*: grey arrow = reduced, black arrow = enhanced bias)[22]. As shown, this closed state associates with a shift from binding of the VSD N-terminus (*red*) with neighboring channels and clustering (*above*) at low K^+ to internal binding that supports the 'locked closed' state and sensitizes channel gating to K^+ (*below*). Mutating the VSD N-terminus yields a channel (mGORK) impaired in both clustering and internal binding, the latter suppressing the 'locked closed' state K^+ inhibition of gating. The mGORK channel thus retains gating characteristics that are closer to the channel clusters, but with a reduced sensitivity to gating inhibition by K^+, that enhances K^+ flux and hence stomatal kinetics.

Fig. 1

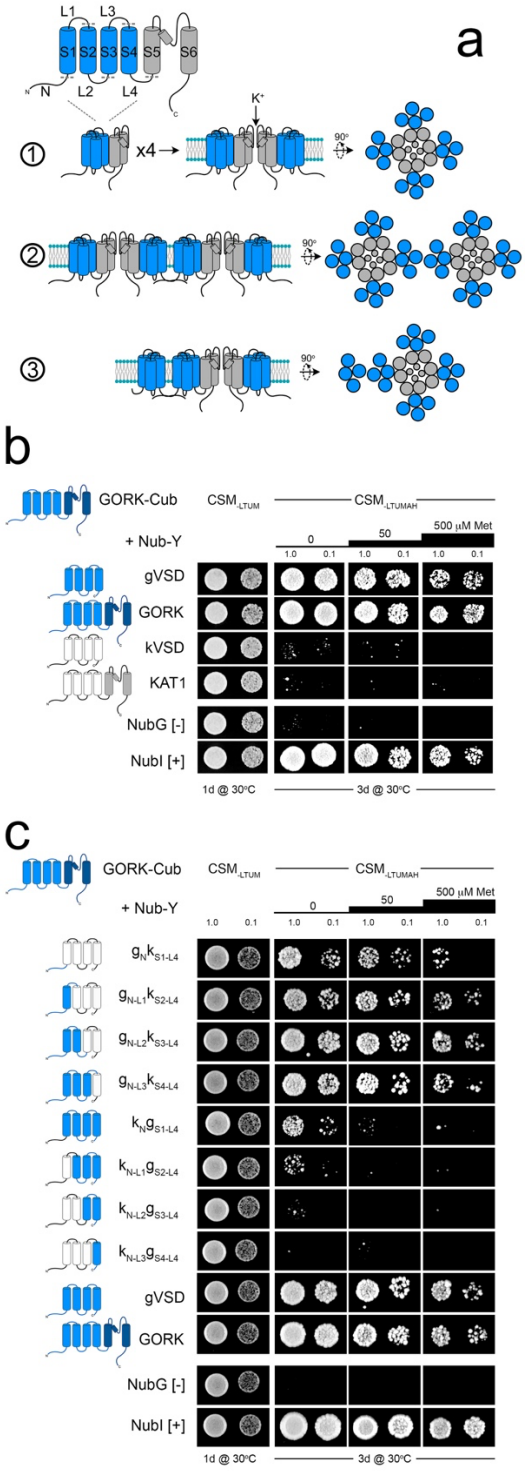
a
L1
L3
S1
S2
S3
S4
S5
S6
N
L2
L4
K+
x4
90°
b
GORK-Cub
CSM-LTUM
CSM-LTUMAH
+ Nub-Y
0
50
500 µM Met
1.0
0.1
gVSD
GORK
kVSD
KAT1
NubG [-]
NubI [+]
1d @ 30°C
3d @ 30°C
c
GORK-Cub
CSM-LTUM
CSM-LTUMAH
+ Nub-Y
0
50
500 µM Met
gNkS1-L4
gN-L1kS2-L4
gN-L2kS3-L4
gN-L3kS4-L4
kNgS1-L4
kN-L1gS2-L4
kN-L2gS3-L4
kN-L3gS4-L4
gVSD
GORK
NubG [-]
NubI [+]
1d @ 30°C
3d @ 30°C

Fig. 2

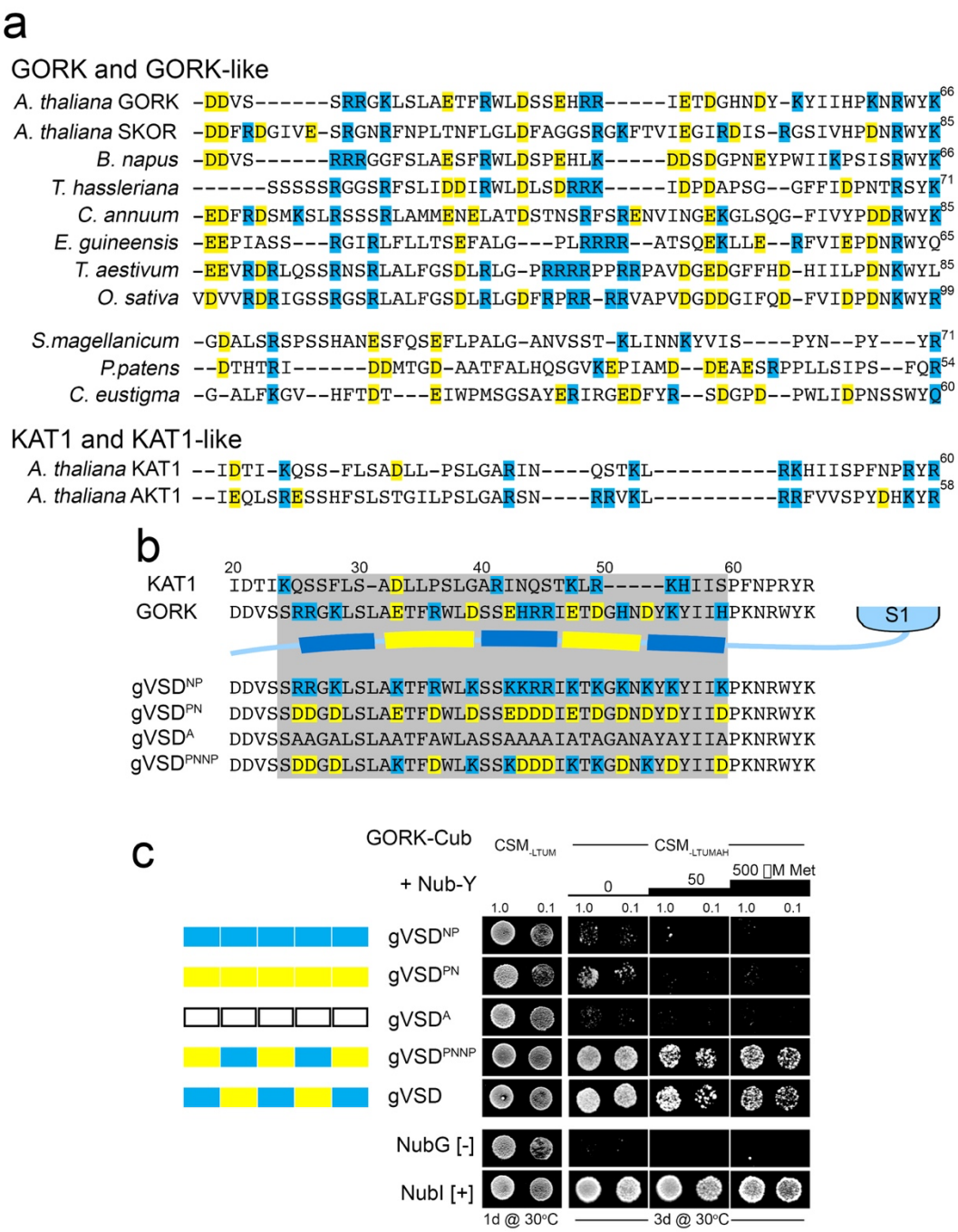
a
GORK and GORK-like
A. thaliana GORK -DDVS------SRRGKLSLAETFRWLDSSEHRR-----IETDGHNDY-KYIIHPKNRWYK 66
A. thaliana SKOR -DDFRDGIVE-SRGNRFNPLTNFLGLDFAGGSRGKFTVIEGIRDIS-RGSIVHPDNRWYK 85
B. napus -DDVS------RRRGGFSLAESFRWLDSPEHLK-----DDSDGPNEYPWIIKPSISRWYK 66
T. hassleriana ------SSSSSRGGSRFSLIDDIRWLDLSDRRK-----IDPDAPSG--GFFIDPNTRSYK 71
C. annuum -EDFRDSMKSLRSSSRLAMMENELATDSTNSRFSRENVINGEKGLSQG-FIVYPDDRWYK 85
E. guineensis -EEPIASS---RGIRLFLLTSEFALG---PLRRRR--ATSQEKLLE--RFVIEPDNRWYQ 65
T. aestivum -EEVRDRLQSSRNSRLALFGSDLRLG-PRRRRPPRRPAVDGEDGFFHD-HIILPDNKWYL 85
O. sativa VDVVRDRIGSSRGSRLALFGSDLRLGDFRPRR-RRVAPVDGDDGIFQD-FVIDPDNKWYR 99
S.magellanicum -GDALSRSPSSHANESFQSEFLPALG-ANVSST-KLINNKYVIS----PYN--PY---YR 71
P.patens --DTHTRI------DDMTGD-AATFALHQSGVKEPIAMD--DEAESRPPLLSIPS--FQR 54
C. eustigma -G-ALFKGV--HFTDT---EIWPMSGSAYERIRGEDFYR--SDGPD--PWLIDPNSSWYQ 60
KAT1 and KAT1-like
A. thaliana KAT1 --IDTI-KQSS-FLSADLL-PSLGARIN----QSTKL----------RKHIISPFNPRYR 60
A. thaliana AKT1 --IEQLSRESSHFSLSTGILPSLGARSN----RRVKL----------RRFVVSPYDHKYR 58
b
20 30 40 50 60
KAT1 IDTIKQSSFLS-ADLLPSLGARINQSTKLR-----KHIISPFNPRYR
GORK DDVSSRRGKLSLAETFRWLDSSEHRRIETDGHNDYKYIIHPKNRWYK
S1
gVSDNP DDVSSRRGKLSLAKTFRWLKSSKKRRIKTKGKNKYKYIIKPKNRWYK
gVSDPN DDVSSDDGDLSLAETFDWLDSSEDDDIETDGDNDYDYIIDPKNRWYK
gVSDA DDVSSAAGALSLAATFAWLASSAAAAIATAGANAYAYIIAPKNRWYK
gVSDPNNP DDVSSDDGDLSLAKTFDWLKSSKDDDIKTKGDNKYDYIIDPKNRWYK
c
GORK-Cub
+ Nub-Y
CSM-LTUM
CSM-LTUMAH
0
50
500 μM Met
1.0 0.1 1.0 0.1 1.0 0.1 1.0 0.1
gVSDNP
gVSDPN
gVSDA
gVSDPNNP
gVSD
NubG [-]
NubI [+]
1d @ 30°C
3d @ 30°C

Fig. 3

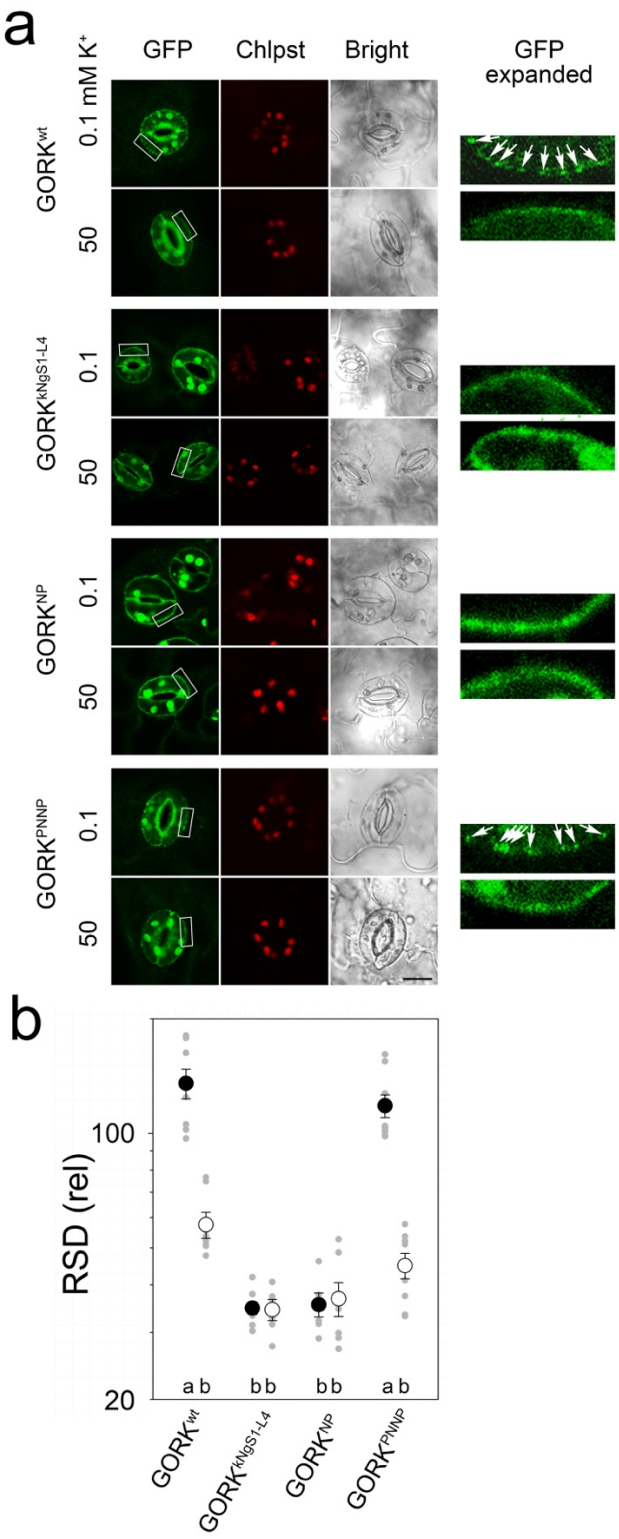
a
GFP
ChlPst
Bright
GFP expanded
0.1 mM K+
GORKwt
GORKKNgS1-L4
GORKNP
GORKPNNP
0.1
50
b
RSD (rel)
100
20
a b
b b
b b
a b
GORKwt
GORKKNgS1-L4
GORKNP
GORKPNNP

Fig. 4

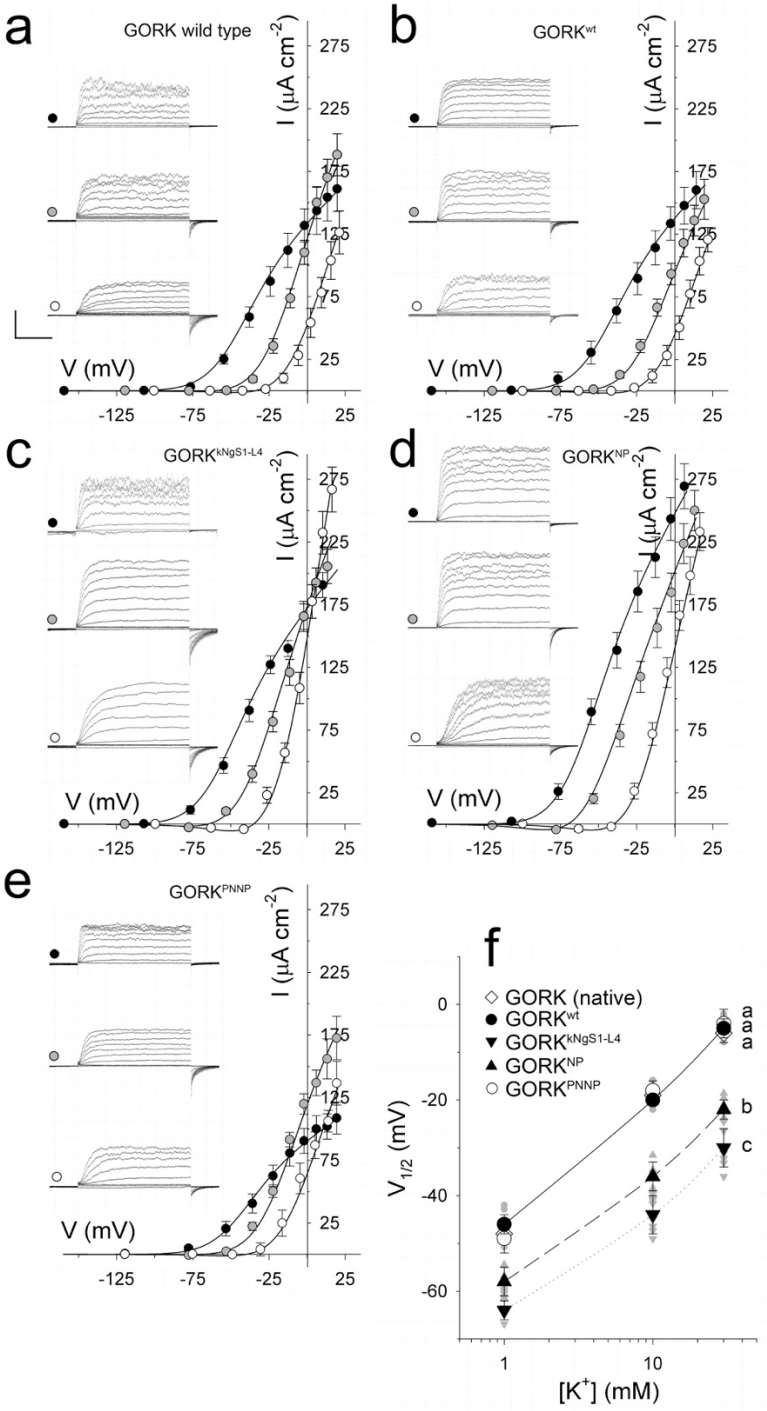
a
GORK wild type
b
GORK^wt
c
GORK^kNgS1-L4
d
GORK^NP
e
GORK^PNNP
I (µA cm^-2)
V (mV)
-125
-75
-25
25
75
125
175
225
275
f
GORK (native)
GORK^wt
GORK^kNgS1-L4
GORK^NP
GORK^PNNP
a
a
a
b
c
V1/2 (mV)
0
-20
-40
-60
1
10
[K+] (mM)

Fig. 5

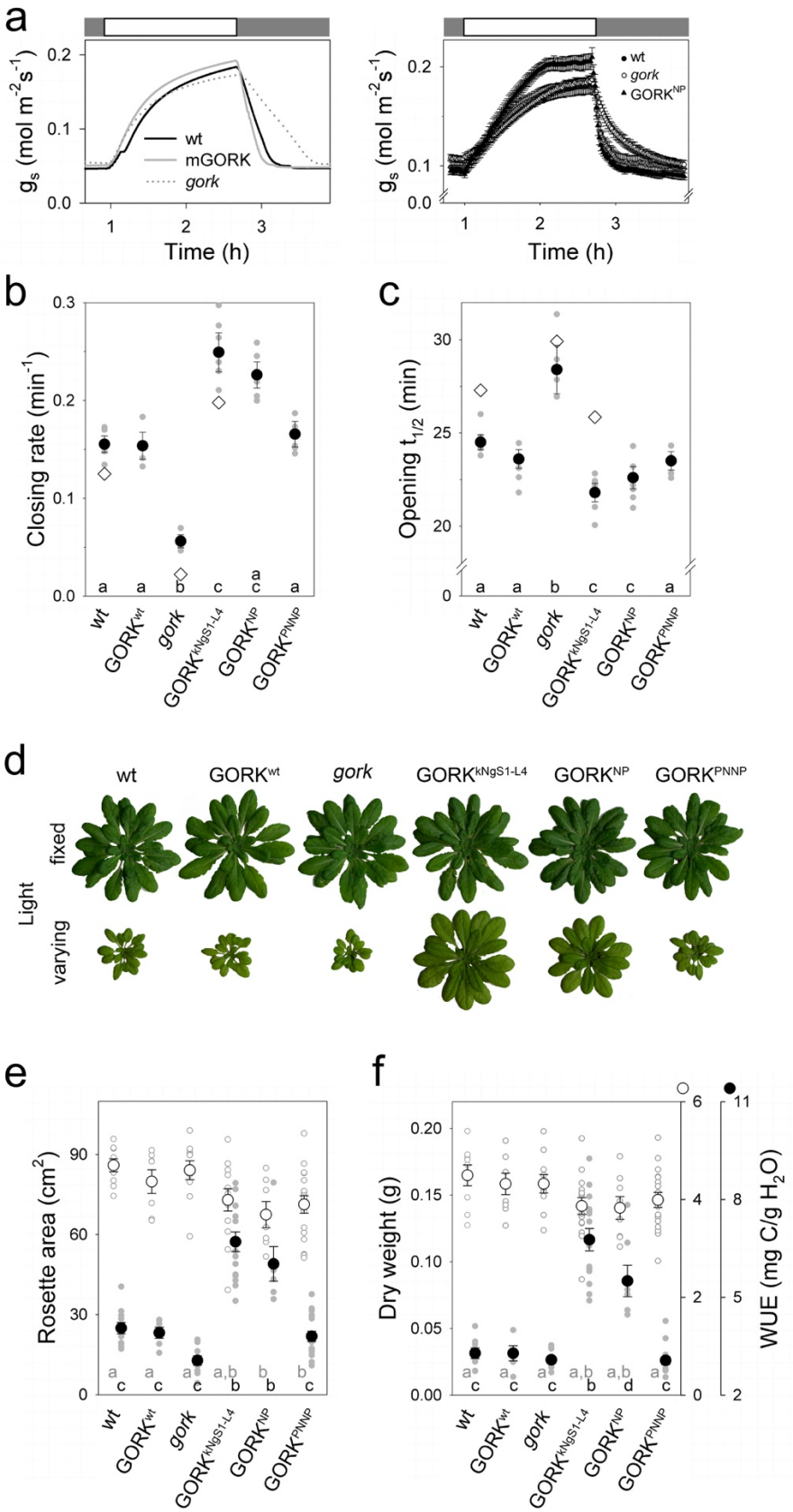
a
g_s (mol m^{-2}s^{-1})
wt
mGORK
gork
Time (h)
wt
gork
GORK^{NP}
b
Closing rate (min^{-1})
c
Opening $t_{1/2}$ (min)
wt
GORK^{wt}
gork
GORK$^{kNgS1-L4}$
GORK^{NP}
GORK^{PNNP}
d
Light
fixed
varying
e
Rosette area (cm^2)
f
Dry weight (g)
WUE (mg C/g H$_2$O)

Fig. 6

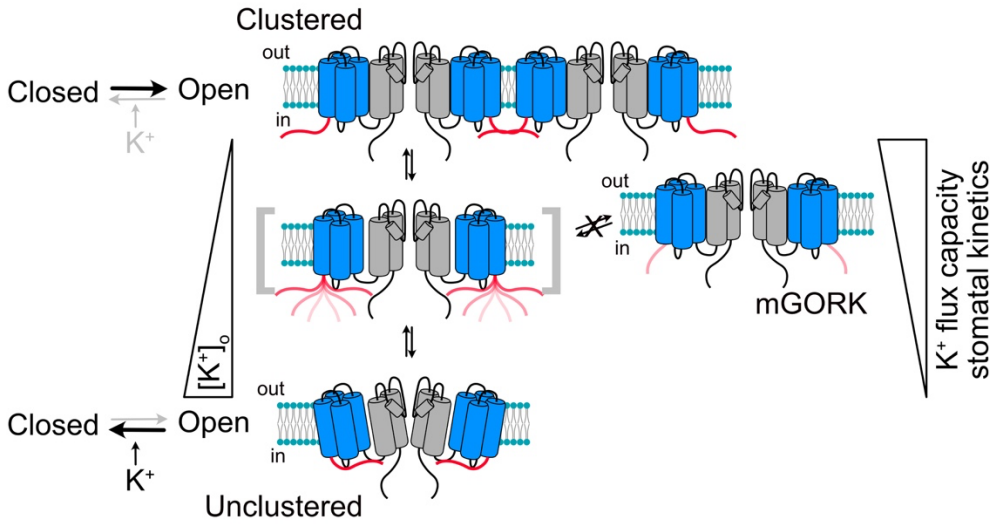
Clustered
Closed
Open
K+
out
in
[K+]o
mGORK
K+ flux capacity
stomatal kinetics
Closed
Open
K+
Unclustered